Available online at www.sciencedirect.com
SCIENCE DIRECT®
Journal of the European Ceramic Society 25 (2005) 857–862
www.elsevier.com/locate/jeurceramsoc

Deformation behaviour of iron-doped alumina

A. Bataille*, A. Addad, J. Crampon, R. Duclos

Laboratoire de Structure et Propriétés de l'Etat Solide, E.S.A.-CNRS 8008, Bât. C6—Cité Scientifique, Université des Sciences et Technologies de Lille, 59655 Villeneuve d'Ascq, Cedex, France

Received 4 June 2003; received in revised form 22 December 2003; accepted 10 January 2004
Available online 20 June 2004

Abstract

Compressive creep tests in air were carried out on 1 cat.% Fe-doped alumina at a temperature $T = 1400\,^{\circ}C$. Iron doping affected the plastic deformation by different ways in relation with Fe^{2+} cations population. Fe^{2+} cations sped up the deformation rates. $FeAl_2O_4$ spinel precipitates were identified and they were found (i) to interact with alumina grain boundaries (ii) to limit the grain growth within a range of strain. The Fe^{2+} cations underwent oxidation and this resulted in the dissolution of the some precipitates and in the decrease of deformation rates. It was suggested that deformation sped up this evolution through mass transport and that time was not a dominating parameter.

Keywords: Al_2O_3; Doping; Creep; Grain size; Grain boundaries

1. Introduction

Useful information can be generated on the nature and on the consequences of ion transport characteristics in alumina and on potential deformation capabilities by studying the effects of substitution impurities on the diffusion creep. The sintering and the creep of transition metals doped alumina have been studied before in terms of defect structure and diffusional processes.[1–7] It has been established that Fe atoms in substitution solid solution change the diffusion properties of alumina.[2,3,5] These effects are related to an enhancement of the cation lattice diffusion (via vacancies and interstitials) with rapid diffusion of oxygen in the grain boundaries.[3] The diffusion changes are associated to the presence of Fe^{2+} cations, which have a relative low solubility in alumina[5,8] whereas Fe^{3+} cations present a large solubility in alumina[9] but have only little influence on the species diffusion properties.[3]

Here, we report the plastic deformation in air of Fe-doped polycrystalline alumina, for a doping level of 1 cat.%, at $T = 1400\,^{\circ}C$ and under different stresses. The plastic deformation presented systematically two sequences: the first one corresponding to a high creep strain rate and the second one following an important decrease of the strain rate. The strain rate change occurred always in the narrow range of compressive true strains [−13%, −17%]. The alteration of strain rate and the grain size evolution have been analysed in terms of porosity, Fe valence evolution, iron aluminate spinel particles precipitation and dissolution.

2. Experimental procedure

The iron-doped alumina was prepared from a high-purity α-alumina powder (SM8, Baikowski, Annecy, France) for which the chemical impurity levels are listed in Table 1. The mean particle size is 0.30 μm.

The powder was mixed with deionised water with the object of obtaining a stable suspension. In order to achieve a homogeneous distribution of iron, aliquots of a high purity $Fe(NO_3)_3{\cdot}6H_2O$ solution were added to the aqueous slurry of alumina powder to yield Fe cation doping level of 1 cat.%. This cation doping level was thought to be large enough to be dominant over the impurity content of the processed powder as listed in Table 2.

The powder was freeze–dried before being calcined in air at $T = 800\,^{\circ}C$ for 2 h to remove nitrogen and possible carbon contaminant. Hot-pressing the calcined powder in vacuum, in a graphite die, for 30 min at 50 MPa produced material discs. The dwelling temperature was 1350 °C. The

* Corresponding author. Tel.: +33-20-434861; fax: +33-20-436591.
E-mail address: Alain.Bataille@univ-lille1.fr (A. Bataille).

0955-2219/$ – see front matter © 2004 Elsevier Ltd. All rights reserved.
doi:10.1016/j.jeurceramsoc.2004.01.006

Table 1
Chemical impurity content of the Baikowski alumina powder

	Na	Si	K	Ca	Cr	Fe
Wt.-ppm	17	38	38	8	4	10

Table 2
Chemical impurity content of the processed alumina powder

	Na	Mg	Si	K	Ca
Wt.-ppm	20	300	100	40	1000

obtained alumina discs had a diameter of 30 mm and a height of 8 mm. The density was measured using the Archimedes' method with methanol as the immersion medium.

Deformation samples were cut from the discs and they had a typical height of 7 mm and a square cross section of $3 \times 3\,\text{mm}^2$. The height was parallel to the hot-pressing axis. Compressive creep tests were carried out in air at $T = 1400\,^{\circ}\text{C}$ and in the true stress range 50–100 MPa. From length change versus time curves, true strain rate versus true strain curves were obtained. A sample was annealed 1200 s at $T = 1400\,^{\circ}\text{C}$, prior to creep testing, to assess the time effect on the evolution of Fe populations and on deformation behaviour.

Microstructure of the different samples were revealed by thermal etching in air at $T = 1400\,^{\circ}\text{C}$ for 1.5 h. The grain sizes (d) were determined, using scanning electron micrograph (SEM) with at least 300 grains counted for each sample, by the relation ($d = 1.38 \times A^{1/2}$),[10] where A is the corrected mean grain surface. The evolution of the grain size during creep under a true stress $\sigma = 75$ MPa was investigated. Reference samples were systematically positioned next to the creeping specimens. This procedure allowed us to observe by SEM the microstructure evolution in a free-strain condition in order to assess the static grain growth. This evolution was compared to the one obtained for the strained specimen, for which both static and dynamic grain growths were active.

Analytical transmission electron microscopy (ATEM, Philips CM30 equipped with an energy dispersive spectroscopy (EDS) Noran X-ray microanalysis) investigations were performed on specimens, which were hot-pressed or crept at different true strains under $\sigma = 75$ MPa.

3. Experimental results

3.1. Compressive creep behaviour

The effect of the compressive true stress on true strain rate behaviour is presented in Fig. 1. Samples exhibited specific deformation behaviour, i.e., a quasi steady state creep was reached during a first stage up to a compressive true strain in the range $\varepsilon = [-13\%, -17\%]$ then, the true strain rate decreased strongly and a second creep stage was observed. Note that the compressive true strain range $\varepsilon = [-13\%, -17\%]$ corresponded to quite different durations according to the applied true stress. Under the true stress $\sigma = 75$ MPa, that time was in a range t (500 s, 1000 s).

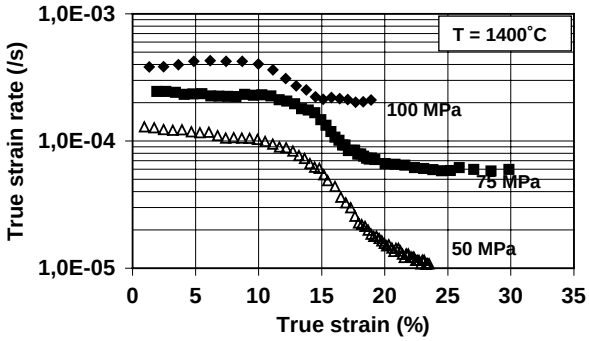

Fig. 1. True strain rate vs. true strain under different true stresses for a 1 cat.% Fe-doped alumina.

For the annealed sample, the annealing time (1200 s) was a bit more than the one corresponding to the time observed to reach the decrease of strain rate in the true strain range $\varepsilon = [-13\%, -17\%]$. No significant difference was observed in its deformation behaviour. The corresponding strain rates were similar and the strain rate belonged to the same true strain range.

3.2. Microstructural features

The hot-pressed materials were densified to more than 98.8% relative density. Fig. 2 presents the microstructure of the hot-pressed materials observed by SEM. Microstructure was homogeneous and the mean grain sizes was 1.6 μm.

Fig. 3 shows the evolution of the mean grain size versus strain. After a short period of grain growth observed at the beginning of the deformation, the grain size remained constant up to about a strain corresponding to the second creep stage. Then the grain grew on. The sample had final

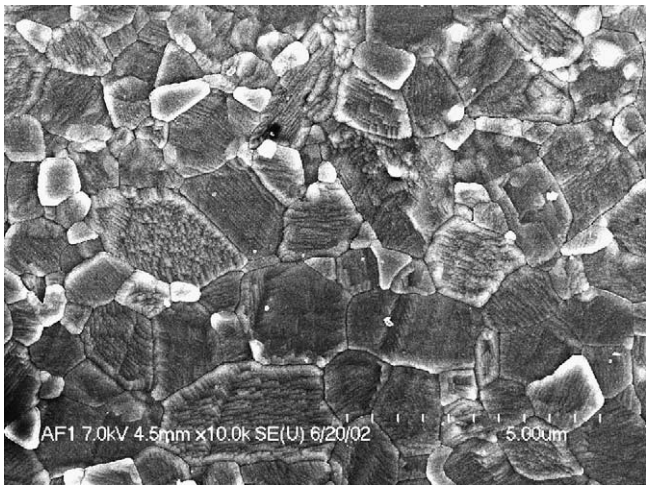

Fig. 2. Microstructure of the as hot-pressed material.

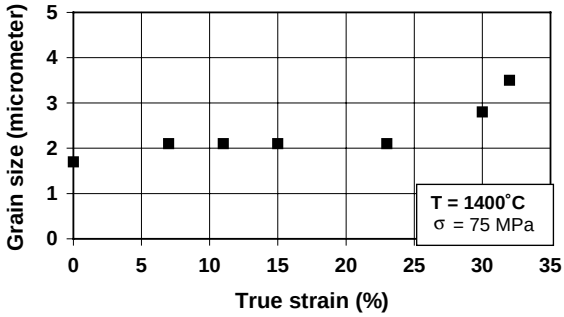

Fig. 3. Evolution of the grain size vs. true strain.

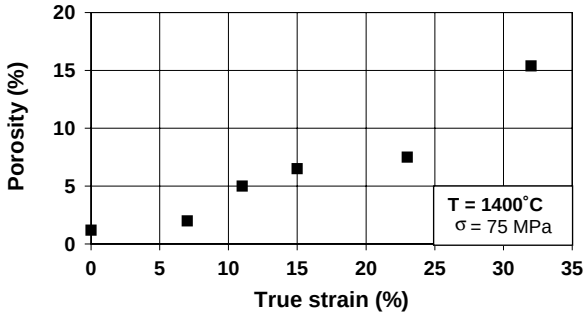

Fig. 4. Evolution of the porosity vs. true strain.

mean grain sizes $d = 3.5\,\mu m$ at true strain $\varepsilon = -32\%$. The microstructure of the reference sample did not evolve in any significant way and the mean grain sizes reached 1.9 μm. Hence the present grain growth, when active, mainly stemmed from the strain effect. In the presented creep conditions, dynamic grain growth dominated. Fig. 4 shows that the porosity increased continuously during creep.

The specimen external colour changed during deformation from an initial dark green colour to a yellowish white. Also the bulk of specimen underwent colour changes from dark green to bright red and eventually yellowish white.

ATEM investigations revealed (i) that iron concentrations higher in the grain boundaries than in the bulk were detected in the hot-pressed material and in the crept specimens, (ii) that iron rich precipitates were present mainly in crept specimens and were located both at grain boundaries and into the grains.

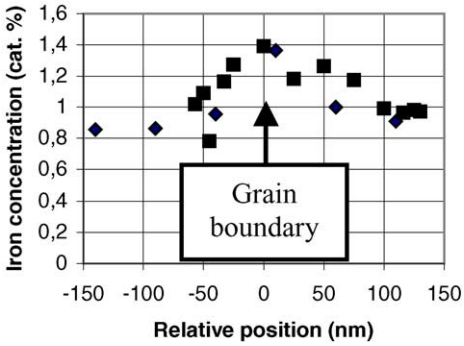

Fig. 6. Fe concentration profile across different grain boundaries in the as hot-pressed alumina.

The chemical mapping of the Fe element shown in the Fig. 5 illustrates this grain boundary enrichment in a deformed sample. In a as hot-pressed sample, the thickness of the iron-richer layer was estimated to be of about 100 nm from the chemical analysis through a grain boundary for which the maximum iron amount was 1.4 cat.% (Fig. 6).

Typical iron-rich precipitates interacting with grain boundaries are shown in Fig. 7, for a specimen deformed up to a true strain $\varepsilon = -11\%$. This precipitation was rarely observed in the as hot-pressed material. From the results of EDS microanalysis, these precipitates were identified as $FeAl_2O_4$ spinel. It should be noted that the chemical identification by ATEM of the tiny Fe-rich particles (less than about 200 nm in apparent size) raises an experimental difficulty in the analysed areas. Indeed, the foil being 30–70 nm thick, when there is a portion of a $FeAl_2O_4$ spinel superimposed on a part of an alumina grain in the foil, the raw composition can correspond to a mixture of chemical compositions of the two phases. The superimposition is avoided for precipitates located at the edge of the thin foil. Hence the experimental difficulty of chemical identification is overcome for those precipitates. Fig. 8 presents such an analysis on a precipitate located at the edge of the thin foil.

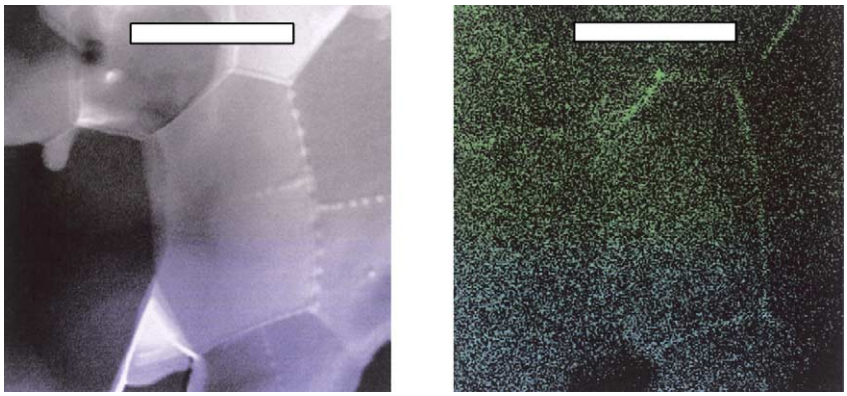

Fig. 5. Mapping of a sample area showing Fe enrichment of grain boundaries in a crept sample ($\varepsilon = -11\%$, $\sigma = 75$ MPa, scale bar: 1500 nm).

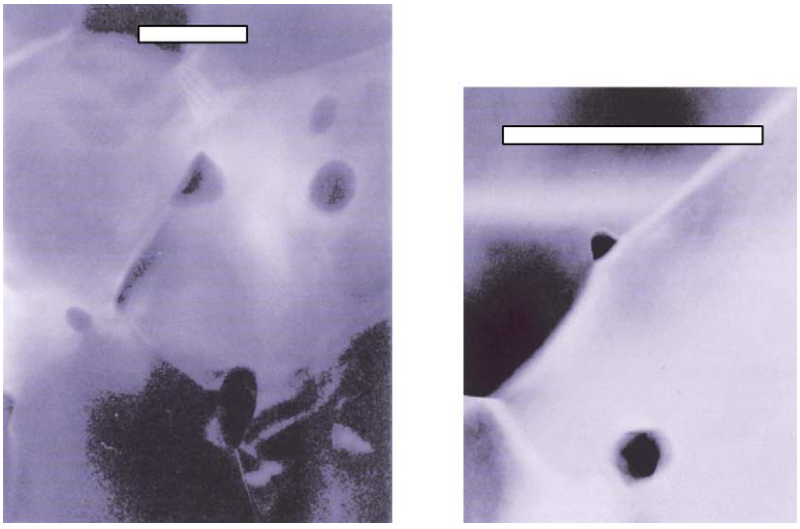

Fig. 7. Pinning of grain boundaries by Fe-rich precipitates in a crept sample and rounded particles into the grains ($\varepsilon = -11\%$, $\sigma = 75$ MPa, scale bar: 1000 nm).

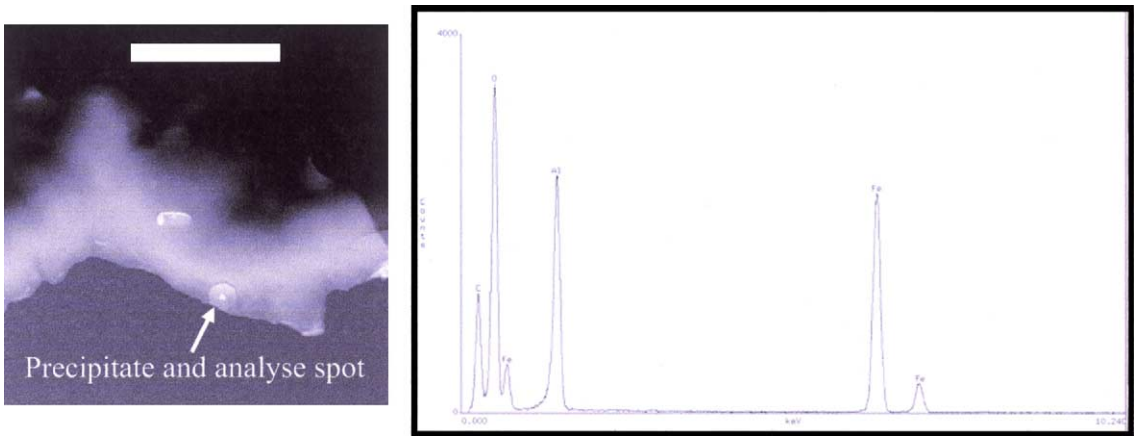

Fig. 8. Microanalysis of a precipitate in a crept sample: the obtained chemical data corresponded to a $FeAl_2O_4$ spinel precipitate ($\varepsilon = -11\%$, $\sigma = 75$ MPa, scale bar: 2000 nm).

4. Discussion

Strain and time are associated to result in the observed specific deformation behaviour. Based on the comparison of the results on crept samples, with and without pre-annealing treatment, it can be concluded that the strain was the dominating factor to explain the experimental creep data. The predominance of the strain effect was also visible through the porosity and grain size evolutions. On one hand, in the pre-annealed sample and in an as hot-pressed sample, respectively, deformed up to similar true strains, respectively, $\varepsilon = -25\%$ and $\varepsilon = -23\%$, the porosity reached similar values $P = 8.1$ and 7.5%. On the other hand, in the present creep conditions, dynamic grain growth was dominating with final mean grain sizes $d = 1.9$ and 3.5 μm, respectively, for the reference sample and for the crept sample.

The most distinctive additional feature found in deformed samples was the precipitation of iron aluminate spinel as a second-phase at grain boundaries. Fig. 3 shows that the grain growth was limited in the true strain range $\varepsilon = [-5\%, -25\%]$. The observed grain boundary/iron aluminate spinel particle configurations show an efficient alumina/alumina boundaries pinning. Consequently the grain growth was temporarily hindered. The rare occurrence of precipitation in the as hot-pressed materials explains presumably the early grain growth, up to a size of about $d = 2$ μm, observed at the beginning of the creep experiments below a true strain of about $\varepsilon = -5\%$ (Fig. 3). Wang and Kröger[11] suggested also about a slowing-down of grain growth in Fe-doped alumina due to the presence of second-phase particles of $FeAl_2O_4$ spinel. Clearly, the volume ratio of the second phase is of importance, but the overall effect must be also related to the distribution and the morphology of the second phase. The more frequent

the occurrence of the particles at grain boundaries, the more effective the grain boundary pinning. The ratio of the second-phase size over the alumina grain size is also an important parameter in the mechanism of grain growth hindrance.[12] When iron aluminate spinel precipitates have formed, some grain boundaries may have overcome the pinning effect of the smaller particles. Consequently, $FeAl_2O_4$ spinel precipitates dragged by alumina boundaries together with intragranular precipitates were to be observed (Fig. 7).

According to Fig. 4, the porosity built up continuously in the deforming specimen. Classically, the interactions between the evenly nucleated pores and the grain boundaries must have also participated in this slowing-down of grain growth.

TEM observations revealed no evidence of any strict correlation between grain boundary cavity nucleation and the presence of a precipitate. Indeed, when second-phase particles were present at alumina grain boundaries, the material might have cavitated during deformation, depending on the diffusion properties of the interface between the two phases. As a matter of example, the SiC nanoparticles at alumina grain boundaries are associated with the nucleation of cavities during deformation[13] due to a strong binding between the two phases. This strong binding must alter the local grain boundary diffusion. It is believed that the iron aluminate spinel precipitates do not largely affect the grain boundary diffusion. Hence, no cavity nucleated at the precipitate–alumina interface in relation to an expected weak binding between alumina and iron aluminate spinel precipitates.

In terms of material transport, the deformation sped up the species diffusion and the material shall not have undergone rapid bulk changes of Fe populations unless crept. The two creep stages observed together with the transient slowing-down of grain growth corresponded to a strain-assisted transition between Fe-based grain boundary segregation to Fe-based precipitation at grain boundaries and to the oxidation of the Fe^{2+} to Fe^{3+}. Eventually both precipitation and oxidation acted during deformation and resulted in the decrease of Fe^{2+} cations concentration. In the present case, it is believed the diffusivity of grain boundaries remained high and the strain rate was maintained as long as the concentration of Fe^{2+} was large enough in the grain boundary vicinity. Hence the shift of strain rate shall be attributed to a concentration of Fe^{2+} falling below a limit and becoming too weak to sustain high grain boundary diffusivity.

From the basis of our observations and results, the discussion will now aim at enlightening the complex role of Fe-doping in the observed deformation behaviour. Hot-pressing at 1350 °C, 30 min in vacuum, in a graphite die, reduced a fraction of the Fe^{3+} cations to Fe^{2+} cations as indicated by the dark green colour of samples. Thus, iron was present in the form of Fe^{2+} cations as well as Fe^{3+} cations in the as hot-pressed alumina. Both cationic populations evolved during deformation. When Fe^{3+} cations had no observed influence on the deformation behaviour of the alumina, Fe^{2+} cations affected this behaviour by multiple ways, i.e., through its solubility, its oxidation to Fe^{3+} cations, and through diffusion of associated defects, precipitation–dissolution processes and second-phase particles/grain boundaries interactions.

The observed enrichment of grain boundary in iron corresponded to the segregation of Fe^{2+} cations. The limited bulk solubility of the Fe^{2+} cations is generally speculated to be low. As a matter of example, Zhao and Harmer[5] estimated the solubility limit of FeO in alumina to be a few hundred of mole ppm at $T = 1620\,^{\circ}C$ in nitrogen. In the present case, the solubility must be even less at $T = 1400\,^{\circ}C$. Any way, it shall be much less than the present Fe doping level.

The rare occurrence of grain boundary precipitation in the as hot-pressed material indicated that the chemical equilibrium was not achieved during the hot-pressing for the final mean grain size $d = 1.6\,\mu m$. This idea has been suggested in the case of transition metal doping of alumina.[14,15] The precipitates must have formed early in the deformation process. It is expected that grain boundary Fe^{2+} concentration has increased during this first step of the creep test corresponding to the initial grain growth. The Fe^{2+} solubility limit of the grain boundary must also be very low, although not known. The enrichment of the grain boundary resulted eventually in the saturation of those grain boundaries for a given grain size, here about 2 μm. From this point on, $FeAl_2O_4$ spinel intergranular precipitates were formed and consequently a grain growth hindrance was temporarily obtained.

The observed specimen external colour change during deformation under air showed a probable change of the Fe^{2+}/Fe^{3+} ratio. As already been reported by Wang and Kröger,[11] the precipitation of iron aluminate spinel is reversible. Due to oxidation, the dissolution of a $FeAl_2O_4$ precipitate phase in $Al_2O_3$was expected according to:

$$O_2 + 4FeAl_2O_4 \rightarrow 2\alpha\text{-}Fe_2O_3 + 4\alpha\text{-}Al_2O_3 \quad (1)$$

A suggestion of an intermediate stage of iron oxidation could be:

$$\tfrac{1}{2}O_2 + 3FeAl_2O_4 \rightarrow Fe_3O_4 + 3Al_2O_3 \quad (2)$$

The solubility of the Fe^{3+} cations is large and when the iron is evenly distributed, at the chemical equilibrium, the final solid solution can be written as $(Fe_2O_3)_x{\cdot}(Al_2O_3)_{1-x}$.

As oxygen diffused rapidly in the grain boundaries, oxidation may have been more active for precipitates located at these boundaries. Resulting from the oxidation, the intergranular pinning iron aluminate spinel precipitates dissolved in alumina during deformation. Then, due to the reduction of the boundary inclusion size, grain boundary mobility was less impeded and grains grew on. As a matter of fact, the alumina grain size was maintained in a limited interval of deformation corresponding to the more frequent observation of intergranular and intragranular $FeAl_2O_4$ spinel precipitates. Moreover, according to our observations, fewer intergranular precipitates were present in the material deformed

up to a true strain $\varepsilon = -23\%$ under $\sigma = 75\,\text{MPa}$. From this strain on, grains grew again.

5. Conclusion

The plastic behaviour of polycrystalline alumina in air has been modified by Fe^{2+}cations doping. Substitution Fe^{2+}cations improved diffusion creep. This beneficial effect was limited due (i) to the low solubility of Fe^{2+}cations in alumina, (ii) to the decrease of the population of substitution Fe^{2+} cations resulting from Fe^{2+} cations precipitation, and (iii) to the oxidation of Fe^{2+}cations population during creep in air.

Also as diffusion was improved, grain growth was eased. This was counterbalanced to some extent by $FeAl_2O_4$ spinel pinning precipitates. Strain was the dominating factor to observe the described deformation behaviour and the iron population changes were strain-assisted.

Acknowledgements

Financial support from the FEDER and from the Conseil Régional Nord/Pas-de-Calais is gratefully acknowledged. The manuscript was improved by the comments of one anonymous referee.

References

1. Rossi, G. and Burke, J. E., Influence of additives on the microstructure of sintered Al_2O_3. *J. Am. Ceram. Soc.* 1973, **56**(12), 654–659.
2. Rao, W. R. and Cutler, I. B., Effect of iron oxide on the sintering kinetics of Al_2O_3. *J. Am. Ceram. Soc.* 1973, **56**(11), 588–593.
3. Lessing, P. A. and Gordon, R. S., Creep of polycrystalline alumina, pure and doped with transition metal impurities. *J. Mater. Sci.* 1977, **12**, 2291–2302.
4. Harmer, P. M., Use of solid solution additives in ceramic processing. In *Advances in Ceramics*, *Vol 10*, ed. W. D. Kingery. Columbus, OH, 1984, pp. 679–696.
5. Zhao, J. and Harmer, M. P., Sintering of ultra-high-purity alumina doped simultaneously with MgO and FeO. *J. Am. Ceram. Soc.* 1987, **70**(12), 860–866.
6. Erkalfa, H., Misirh, Z., Demirci, M., Toy, C. and Baykara, T., The densification and microstructural development of Al_2O_3 with manganese oxide addition. *J. Eur. Ceram. Soc.* 1995, **15**, 165–171.
7. Xue, L. A. and Chen, I. W., Superplastic alumina at temperatures below 1300 °C using charge compensating dopants. *J. Am. Ceram. Soc.* 1996, **79**(1), 233–238.
8. Novokhatskii, I. A., Belov, B. F., Gorokh, A. V. and Savinskaya, A. A., The phase diagram for the system ferrous oxide-alumina. Russ. *J. Phys. Chem.* 1965, **39**(11), 1498–1499.
9. Muan, A., On the stability of the phase $Fe_2O_3{\cdot}Al_2O_3$. *Am. J. Sci.* 1958, **256**(6), 413–422.
10. Carry, C. and Mocellin, A., Structural superplasticity in single phase crystalline ceramics. *Ceram. Int.* 1987, **13**, 89–98.
11. Wang, H. A. and Kröger, F.A., Pore formation during oxidative annealing of Al_2O_3–Fe and slowing of grain growth by precipitates and pores. *J. Mater. Sci.* 1980, **15**, 1978–1986.
12. Duclos, R. and Crampon, J., Grain boundary-inclusion interactions in a zirconia-alumina ceramic composite. *Scripta Met. Mater.* 1990, **24**, 1825–1830.
13. Ohji, T., Nakahira, A., Hirano, T. and Niihara, K., Tensile creep behaviour of alumina/silicon carbide nanocomposite. *J. Am. Ceram. Soc.* 1994, **77**(12), 3259–3262.
14. Li, C.W. and Kingery, W.D., Solute segregation at grain boundaries in polycrystalline Al_2O_3. In *Advances in Ceramics, Vol 10*, ed. W. D. Kingery. Columbus, OH, 1984, pp. 368–378.
15. Gruffel, P., Ph.D. Thesis. 921, EPFL, Lausanne, Switzerland, 1991.